Materials Science & Engineering A 835 (2022) 142665

Contents lists available at ScienceDirect

Materials Science & Engineering A

journal homepage: www.elsevier.com/locate/msea

Mechanical properties and crystallographic texture of non-oriented electrical steel processed by repetitive bending under tension

Saeed Tamimi [a,*], Youliang He [b], Mehdi Sanjari [b,c], Hadi Pirgazi [d], Winfried Kockelmann [e], Fiona Robinson [f], Mohsen Mohammadi [c], Leo Kestens [d]

[a] Advanced Forming Research Centre (AFRC), University of Strathclyde, Glasgow, United Kingdom
[b] CanmetMATERIALS, Natural Resources Canada, Hamilton, ON, Canada
[c] Marine Additive Manufacturing Centre of Excellence (MAMCE), University of New Brunswick, Fredericton, NB, Canada
[d] Department of Electromechanical, Systems and Metal Engineering, Ghent University, Ghent, Belgium
[e] Science and Technology Facilities Council (STFC), Rutherford Appleton Laboratory, ISIS Facility, Harwell, United Kingdom
[f] School of Engineering, University of South Wales, Treforest, Pontypridd, United Kingdom

ARTICLE INFO

Keywords:
Non-oriented electrical steel
Repetitive bending under tension
Continuous bending under tension
Recrystallisation
Crystallographic texture

ABSTRACT

Improving the magnetic properties of non-oriented electrical steel (NOES) through the optimization of crystallographic texture has been an on-going research activity for decades. However, using traditional rolling and annealing procedures, the obtained final textures were usually very similar, i.e., exhibiting the {111} (γ) and <110> (α) fibres, which were not the desired {001} texture (θ-fibre) for optimal magnetic quality. In the current work, a 1.8 wt% Si NOES was processed using a new sheet metal deformation method, i.e., *repetitive bending under tension* (R-BUT), also known as *continuous bending under tension* (C-BUT), to modify the texture of the electrical steel. The hot-rolled and annealed NOES plates were repeatedly bent and unbent when they were pulled under tension. The deformed plates were then heat treated at different temperatures for various times. Neutron diffraction and electron backscatter diffraction (EBSD) characterisation of the macro- and micro-textures proved that the R-BUT process significantly reduced the undesired {111} texture while promoting the {001} texture. The cube texture, which rarely formed after conventional rolling and annealing, was also seen in the R-BUT samples after annealing. It was shown that, the shear plastic deformation (induced by R-BUT) played a significant role in promoting the desired textures. In addition, the results indicated that the NOES processed by R-BUT could be deformed beyond its common formability limit, which may provide a method to address the poor workability challenge of high silicon electrical steels.

1. Introduction

Electrical steels, also known as silicon steels, are widely used as soft magnetic cores in electric motors (e.g. for rotating machines and electric vehicles), generators, alternators, etc. These steels are normally manufactured through hot rolling, hot band annealing, cold rolling, and final annealing, to form thin sheets for core lamination. Electrical steels usually contain a large amount of silicon (normally up to 3.5 wt%, maybe as high as 6.5 wt%) since silicon increases the electrical resistivity (resulting in a reduction in the eddy current loss) and decreases the magnetic anisotropy, which are favourable for electric motors. Due to the extremely large number of electric motors used in many fields, even small improvement in the electrical and magnetic performance of the NOES may have a significant impact on the overall energy consumption. For example, in the automotive industry, increasing the efficiency of the traction motors of electric vehicles can lead to an extended driving range under the same battery capacity, which can help resolve the range anxiety issue of electric vehicles.

Once the silicon content is determined and the required sheet thickness is achieved, the microstructure and crystallographic texture are the most important factors which control the core loss and the magnetic permeability of the NOES sheets. A uniform grain shape throughout the sheet thickness with an average grain size of approximately 150 μm is desired [1]. The microstructure and texture after final annealing are the most critical metallurgical factors affecting the magnetic quality of the steel. These are not only dependent on the

* Corresponding author.
E-mail address: saeed.tamimi@strath.ac.uk (S. Tamimi).

https://doi.org/10.1016/j.msea.2022.142665
Received 2 November 2021; Received in revised form 9 January 2022; Accepted 10 January 2022
Available online 13 January 2022

parameters used in the final heat treatment operation, but also closely related to those applied in the previous processing steps, e.g. hot rolling, hot band annealing, cold rolling, intermediate annealing, etc. It has been shown in [2] that, shear plastic deformation together with annealing can promote the development of the cube texture ({001}<100>), which is a desired texture in NOES since it has two easy magnetization crystallographic directions in the sheet plane.

It has also been reported that alternative rolling processes such as asymmetric rolling (ASR) [3], cross rolling [4], inclined rolling [5,6], and skew rolling [7,8], would be able to develop favourable textures in NOES sheets. The impact of ASR parameters on shear plastic deformation has been reported in several studies, see e.g. [9,10]. In addition, it has been shown that the change in the level and direction of shear plastic deformation through cold ASR could alter the microstructure and texture of ferritic steel sheets [11]. The introduced shear plastic deformation together with the subsequent recrystallisation can assist in the development of the desired texture for magnetic applications [2].

Repetitive bending under tension (R-BUT) is another promising method to introduce shear plastic deformation throughout the sheet thickness [12,13]. This process is also known as continuous bending under tension in previous works, e.g. [14]. This shear plastic deformation can refine the grains as well as develop favourable textures after annealing. Another feature of R-BUT is that this process can deform the materials far beyond their common elongation limits, as has been shown in previous studies [15]. This is especially beneficial to materials with low ductility, i.e., electrical steels with high silicon contents. Hence, this study is intended to investigate how the R-BUT process can assist in developing the desirable microstructure and crystallographic texture in electrical steel. A NOES containing 1.8 wt% of Si was processed by R-BUT at room temperature. The microstructure and texture evolution is evaluated using EBSD and neutron diffraction techniques. The impact of the R-BUT deformation on the formation of the recrystallisation microstructure and texture is investigated.

2. Material and experimental procedure

The chemical composition of the NOES used in this work is (wt%): 1.826 Si, 0.0023 C, 0.299 Mn, 0.515 Al, 0.010 P and 0.001 S. The steel was melted in a vacuum induction furnace and then cast into a 200 mm × 200 mm ingot (~227 kg). After preheating to ~1038 °C, the ingot was hot rolled to about 25 mm thick in a two-high reversing rolling mill in 6 passes. After removing the oxide layers (~3 mm on each side), the plate

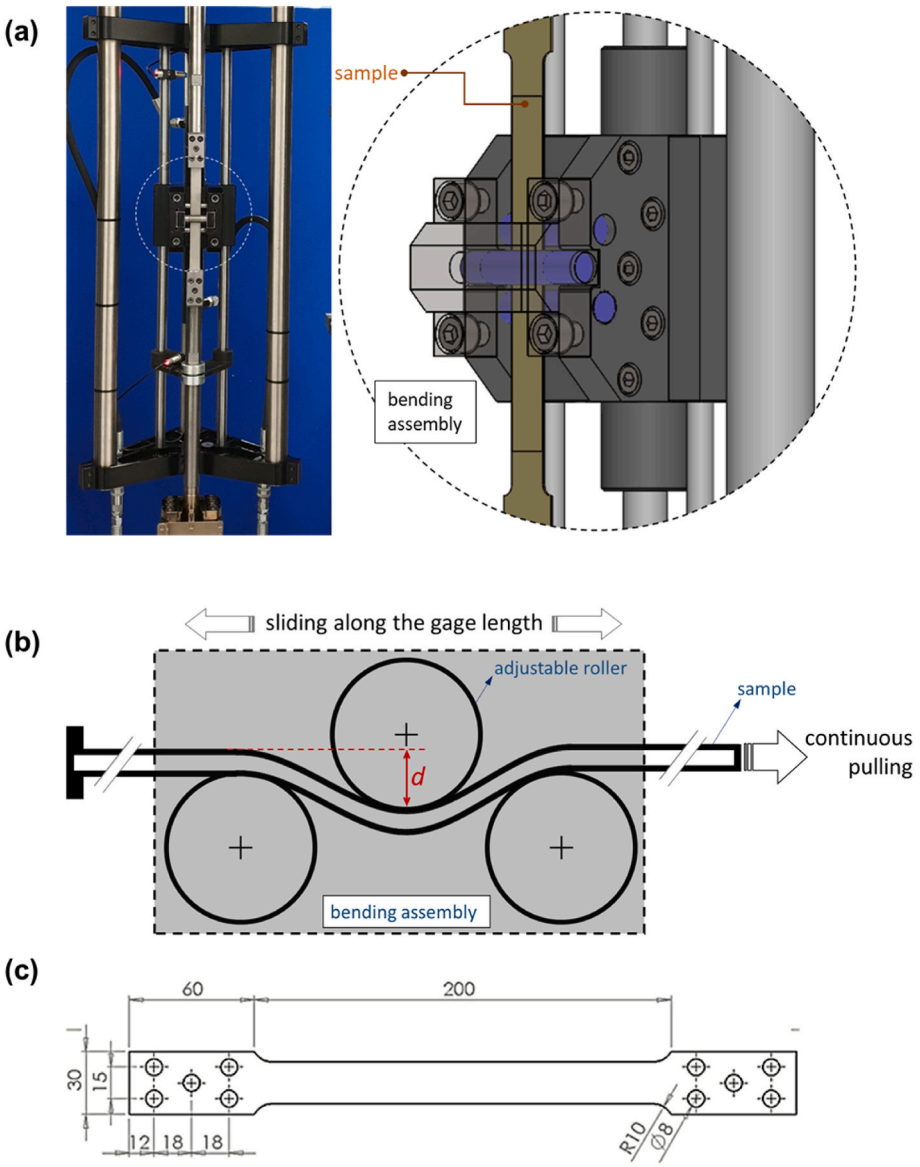

Fig. 1. Experimental setup: (a) photograph of the R-BUT testing assembly, and (b) schematic of the bending assembly, (c) R-BUT testing specimen.

was reheated again to ~1038 °C and further hot rolled to ~2.3 mm. The hot-rolled plates were pickled in hydrochloric acid and annealed at ~840 °C for 60 h in 100% dry hydrogen [7]. Strips of 320 mm × 30 mm (RD × TD) were then waterjet cut from the annealed plates for R-BUT deformation. The cold-deformed samples were final annealed to obtain recrystallised microstructures. The testing rig of the R-BUT process is shown in Fig. 1a and b, and the geometry of the R-BUT specimens are given in Fig. 1c (the dimensions are in mm). The details of the testing procedure have been described elsewhere [15], and can be briefly summarized below:

a) Insert the testing specimen into the rig and grip the two ends to the tensile machine.
b) Apply bending deformation to the sample through the adjustable roller (Fig. 1b).
c) Apply pulling (tension) load and simultaneously move the bending assembly up and down with a controlled velocity.

The prominent R-BUT parameters that influence the material deformation include the level of bending (penetration depth), the movement speed of the bending assembly, and the pulling velocity. Since the strain rate is a function of both the pulling velocity and the velocity of the bending assembly, a parameter ω is used to describe the straining, which is defined as the ratio of these two speeds, i.e.

$$\omega = \frac{bending\ assembly\ velocity\ (mm/s)}{pulling\ velocity\ (mm/s)} \quad (1)$$

Table 1 lists the R-BUT testing parameters used in this study. Two main parameters were varied, i.e., the speed ratio ω and the penetration depth d (the distance of the adjustable roller penetrated into the static rollers, as shown in Fig. 1b). A greater velocity ratio means a larger ratio of the shear strain to the tensile strain. A larger penetration depth leads to a higher bending level, i.e. a smaller bending radius. The R-BUT operations were carried out at room temperature. Full lubrication was applied to minimize the surface damage caused by tooling contact. In order to evaluate the uniformity of the thickness reduction along the gauge length of samples during the R-BUT process, a non-contact blue-light 3D scanning technique was used to measure the sample thickness, and the data was analysed using the GOM ATOS® software.

The texture was characterized by both neutron diffraction (macro-texture) and electron backscatter diffraction (microtexture). For neutron diffraction, samples of 8 mm × 15 mm (TD × RD) were prepared from both the annealed hot band (before R-BUT deformation) and the R-BUT deformed strips. The data were collected on the General Material (GEM) neutron diffractometer at the ISIS pulsed neutron spallation source, UK [16] using a polychromatic neutron beam with neutron wavelengths between 0.2 and 3.5 Å. A sample was mounted in a vacuum chamber and a data for one sample orientation was collected. The data analysis was conducted by the Rietveld method with the MAUD [17] analysis package for neutron time-of-flight data. The orientation distribution functions (ODFs) were plotted using the MTEX software [18]. For EBSD characterisation, selected samples were cut and mounted, and mechanically ground and polished to mirror finish followed by a final step of vibro-polishing for a maximum of 120 min. The EBSD patterns were acquired using a field-emission gun scanning electron microscope (FEI Quanta-650), with an accelerating voltage of 20 kV. The data were analysed using the orientation imaging microscopy (OIM) software package. The crystallographic texture was shown using ODFs on the φ_2 = 0° and 45° sections (Bunge notation) since all the important texture components and fibres for body centred cubic (bcc) iron fall in these sections. To facilitate the identification of major texture components and interpret the change of texture, typical texture components and fibres in these sections are shown in Fig. 2.

Table 1
Parameters used in the R-BUT tests.

	Set 1	Set 2	Set 3	Set 4	Set 5
Penetration Depth: d (mm)	1	2	2	2	4
Velocity Ratio ω :	800	400	800	2000	400

3. Results

3.1. Microstructure and texture before R-BUT

The EBSD results of the annealed hot band (before R-BUT) are presented in Fig. 3. The scan was taken on the ND-RD plane across the entire sheet thickness. The microstructure contains equiaxed grains with a heterogeneous distribution of grain sizes, i.e. small grains with diameters of tens of microns and large grains of hundreds of microns coexist; the average grain size is ~265 μm. Generally, the grains near the surfaces are smaller than those in the middle. The prominent microtexture is the θ-fibre (<001>//ND), with peaks at cube ({001}<100>) and {001}<130>. Components such as {113}<110>, {112}<110> and {225}<142> on the $\varphi_2 = 45°$ section are also noted.

The macrotexture of the annealed hot band measured by neutron diffraction (through the entire thickness) is shown in Fig. 4a. The texture is quite weak, with a maximum intensity of only 2.2. The cube component observed in the microtexture (Fig. 3) is not seen in the macrotexture. The strongest components are close to Goss and rotated cube. There is essentially no <111>//ND (γ-fibre) or <110>//RD (α-fibre). The neutron diffraction texture is also different from the texture measured by X-ray diffraction at the middle thickness plane (Fig. 4b), where {001}<120> and {113}<361> are the main components, together with a <111>//ND fibre (as reported previously on the same steel [7]). It is noted that, the texture at the middle-thickness plane (maximum intensity of 8.7) is much stronger than the texture through the thickness as measured by neutron diffraction. The differences in texture measured by EBSD, X-ray diffraction and neutron diffraction were mainly due to the differences in the sampling locations and the number of grains covered. The EBSD scan only covered a small area (2.3 mm × 2.6 mm) across the thickness, which included a few hundred grains only. The X-ray diffraction covered an area of about 10 mm × 15 mm, but it only measured the texture on the middle thickness plane of the steel plate. The neutron diffraction covered an 8 mm × 15 mm area, and it was through the entire plate thickness covering a larger number of grains. Therefore, it is the best representation of the bulk texture of the material.

3.2. Mechanical behaviour of the NOES under R-BUT

The influence of the velocity ratio (ω) on the mechanical behaviour of the NOES subjected to R-BUT is shown in Fig. 5a, where the penetration depth (d) for all the R-BUT samples is the same (2 mm). Compared to standard tensile test, an outstanding feature of the R-BUT process is that the tensile force needed to deform the material is significantly reduced, i.e., only about 1/4 of that of standard tensile test (Fig. 5b), while the elongation can be increased by up to 4 times. The overall strain hardening for all three R-BUT specimens follow the same trend, but the required tensile force generally decreases with the increase of ω. Nevertheless, when the velocity ratio (ω) increases to 800 or higher, the required tensile force only slightly decreases. On the other hand, with the increase of ω, the elongation is gradually reduced. This means that, when the velocity ratio is greater than 800, there is only very small reduction on the tensile force, but with a large decrease in the formability of the material.

It is worth mentioning that the R-BUT samples under various velocity ratios failed after different numbers of R-BUT cycles due to fracture, i.e., $\omega = 400$, 68 cycles, $\omega = 800$, 124 cycles, $\omega = 2000$, 308 cycles. There is a linear relationship between the velocity ratio and the number of R-BUT cycles after which the specimen failed (Fig. 5c). For the ω = 2000

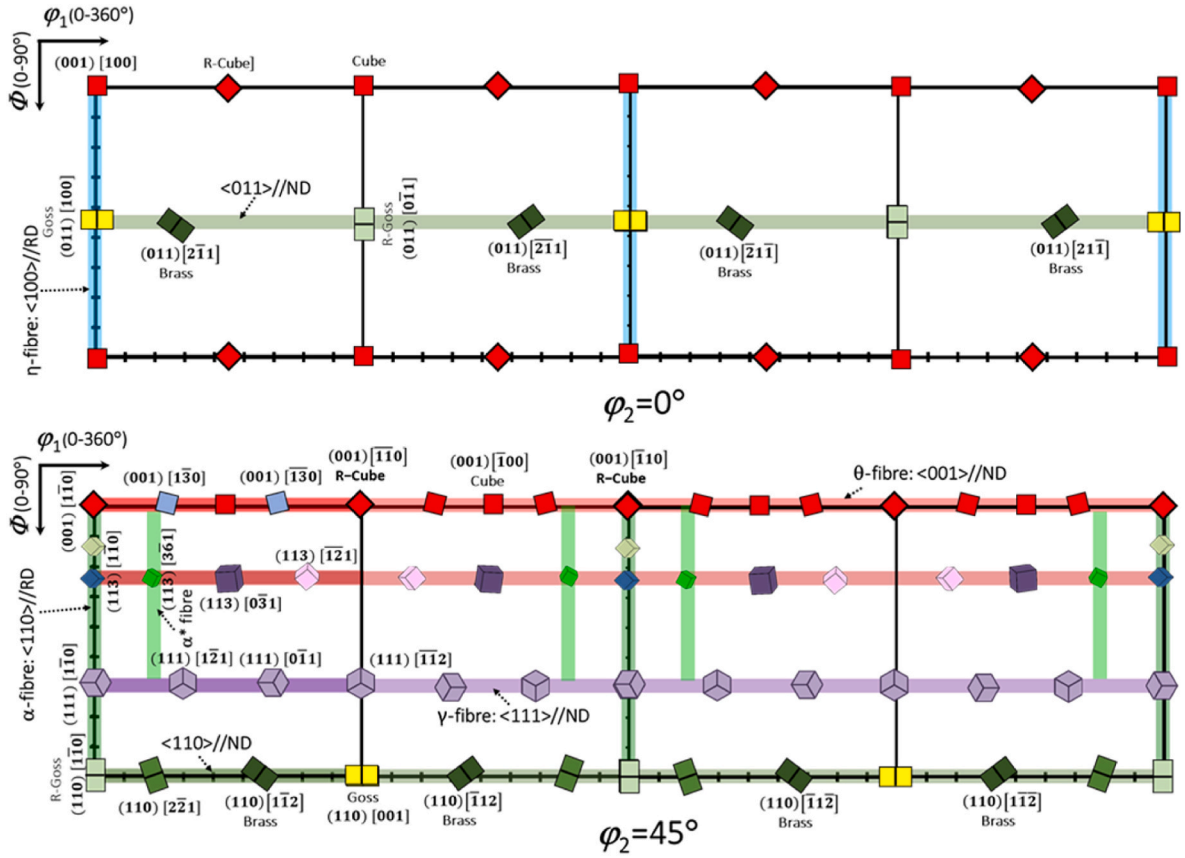

Fig. 2. Typical texture components and fibres in bcc materials as displayed in $\varphi_2 = 0^\circ$ and 45° ODF sections (Bunge notation).

sample, each point of the sample within the gage length has been bent and unbent for 616 times when the bending package slides up and down. This large number of R-BUT cycles for the case with the highest ω was associated with the lowest level of tensile straining applied on the sheet during the test.

The effect of the penetration depth (d) on the load-displacement curve of the NOES specimens subjected to R-BUT is shown in Fig. 6. As mentioned before, the penetration depth can be translated into the bending levels: the larger the penetration depth, the larger the bending level. For both $\omega = 400$ and $\omega = 800$, the maximum tensile force significantly decreases with the increase of the bending level (penetration depth), so does the elongation. During bending, a part of the sheet is under tension whereas the other part is under compression. The tension and compression parts are separated by the neutral plane in the sheet. The process parameters determine the location of the neutral plane. The tensile loading required to deform the R-BUT testing piece depends on the area in the cross-section where the material is under compression [19]. Fig. 6 illustrates that the higher the bending level, the lower the tensile load required. For these specimens, higher portions of material within the cross-section are under compressive strain, which causes less forces required for deformation. When the material is being bent and unbent through the R-BUT operation, the material requires less tensile force to plastically deform the material as compared to the standard yield strength under conventional tensile load. As a result, the rest of the material which is under lower forces than the yield strength remains elastic. Fig. 6c shows a photograph of an actual R-BUT tested sample (Set 1) along with the measured thicknesses after the R-BUT process. The surface colour plot shows that the R-BUT sample demonstrated a fairly uniform reduction along the gauge length, suggesting a relatively stable flow of the material under the R-BUT conditions.

3.3. Microstructure and crystallographic texture

Microstructure and crystallographic texture of the specimen subjected to R-BUT under a penetration depth of $d = 2$ mm and $\omega = 400$ are presented in Fig. 7. The inverse pole figure (IPF) map (Fig. 7a) shows that the microstructure consists of grains with various orientations, but the <101>//ND (green) and <113>//ND (pink and purple) grains dominate the microstructure. Kernel average misorientation (KAM) analysis (Fig. 7b) illustrates that the {113} grains generally have larger misorientation angles, indicating larger deformation within these grains. Shear bands are also visible in these grains, which are due to the accumulation of highly localised dislocations caused by non-uniform deformation [20]. These shear bands are associated with the shear plastic deformation occurring during the R-BUT. The {101} grains, on the other hand, generally deform more uniformly with relatively low KAM. The distribution of the misorientation angles of the sample before and after R-BUT is shown in Fig. 7c, which indicates that the majority of the grain boundaries after R-BUT have low misorientation angles (<10°) whereas most grain boundaries of the specimen before R-BUT have high misorientation angles (≥20°), with a maximum fraction around 45°. The microtexture of the scanned area is given in Fig. 7d, which shows textures such as <113>//ND, <101>//ND and <111>//ND.

Fig. 8 shows the bulk texture (macrotexture) of the same sample measured by neutron diffraction. The overall intensity of the texture is also very small, i.e., with a maximum intensity of ~2.0. The macrotexture is dominated by a rotated cube, an α-fibre, a near (parallel to) γ-fibre, and a weak Goss component. These are quite similar to the typical textures after cold rolling. There is an apparent discrepancy between the micro- and macro-textures: the strong rotated cube observed in the macrotexture does not appear in the microtexture, while the brass ({101}<121>) component observed in the microtexture is not seen in the macrotexture. These differences are due to the small number

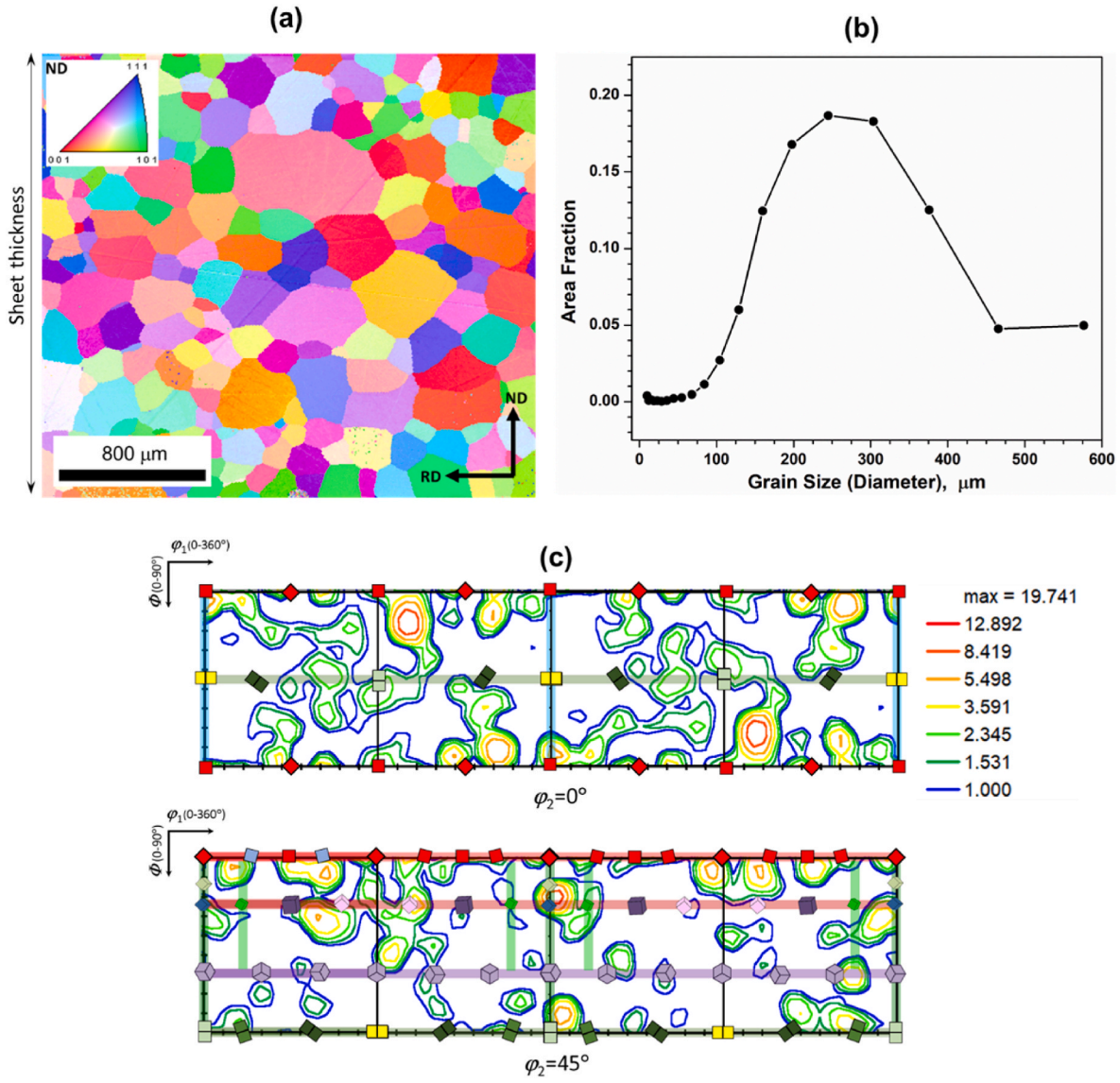

Fig. 3. EBSD analysis of the hot-band-annealed electrical steel: (a) inverse pole figure map; (b) grain size distribution; (c) microtexture shown on $\varphi_2 = 0^\circ$ and 45° ODF sections.

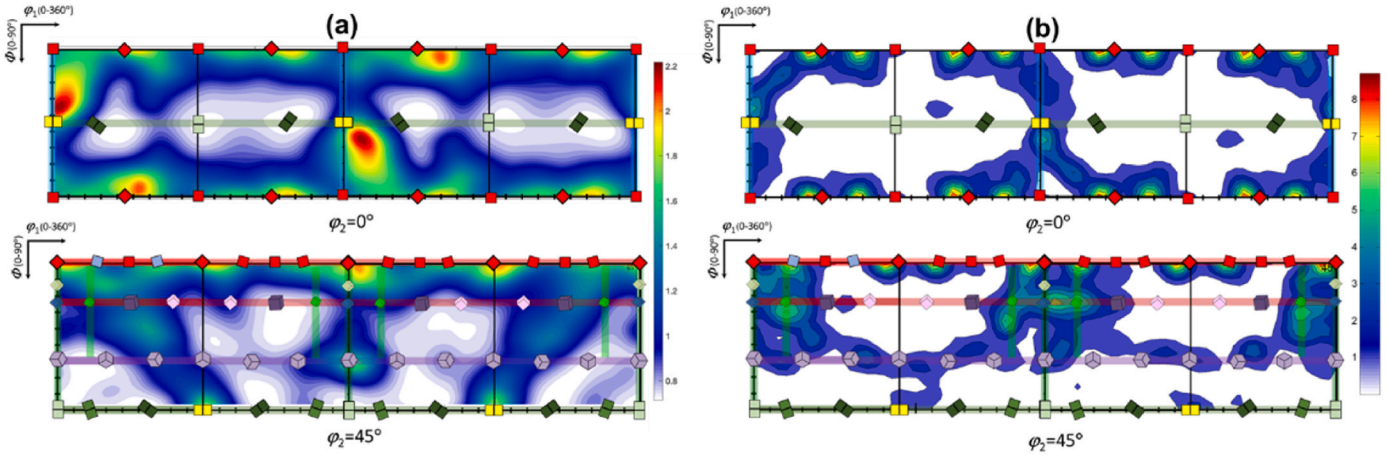

Fig. 4. Macro-textures of the annealed hot band measured by: (a) neutron diffraction through the entire thickness, (b) X-ray diffraction on the middle-thickness plane [7].

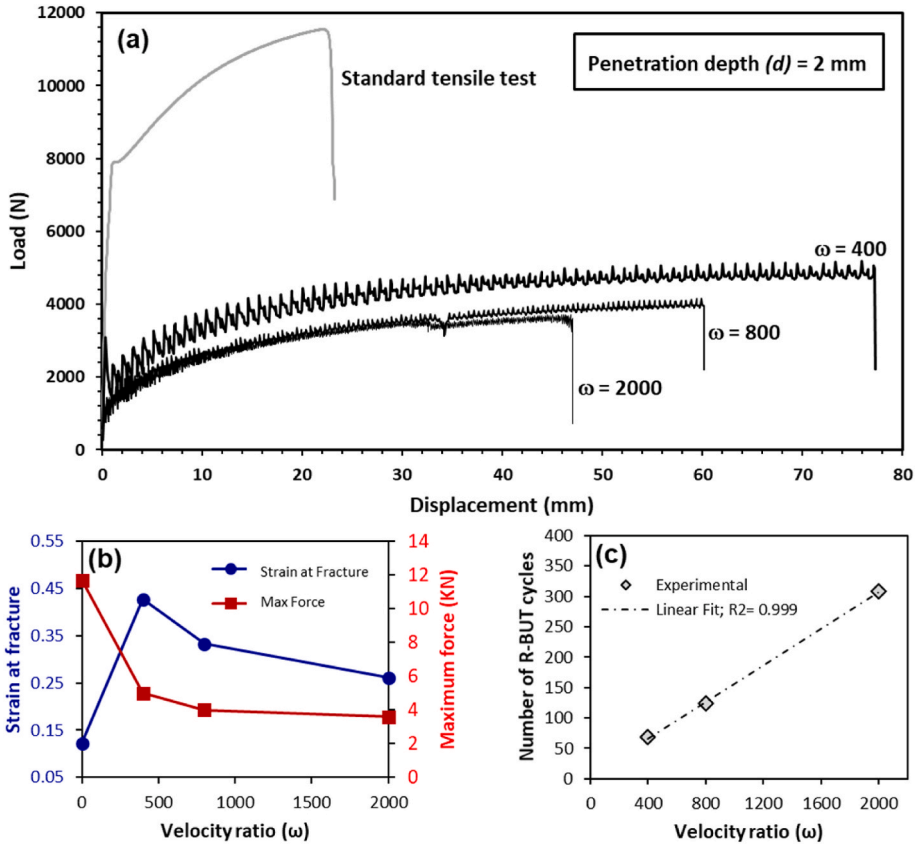

Fig. 5. The influence of ω on R-BUT characteristics: (a) the load-displacement curves of hot-band-annealed NOES subjected to R-BUT, (b) the corresponding maximum force and fracture strains, (c) the relationship between the velocity ratio and the number of R-BUT cycles before the specimen failed.

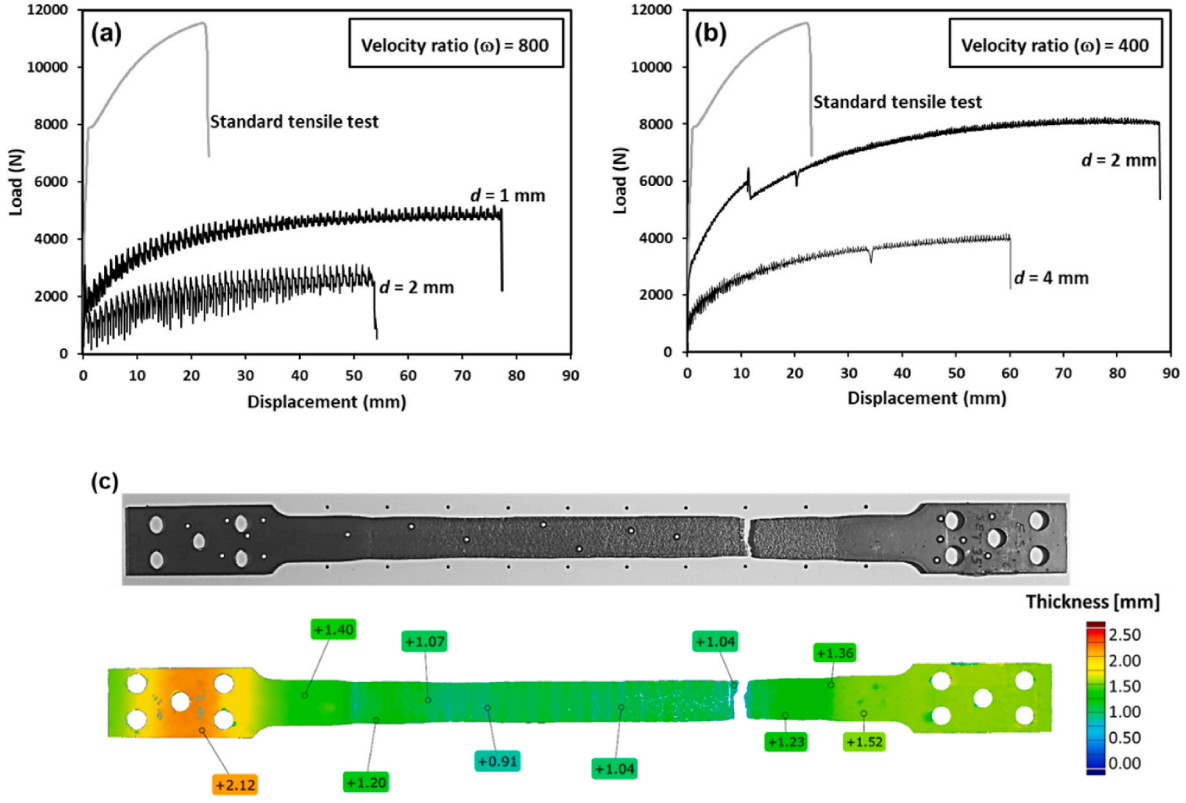

Fig. 6. The Influence of bending level on the load-displacement curves of hot-band-annealed NOES subjected to R-BUT: (a) velocity ratio = 800, (b) velocity ratio = 400, (c) photograph of an R-BUT processed sample and the variations in thickness.

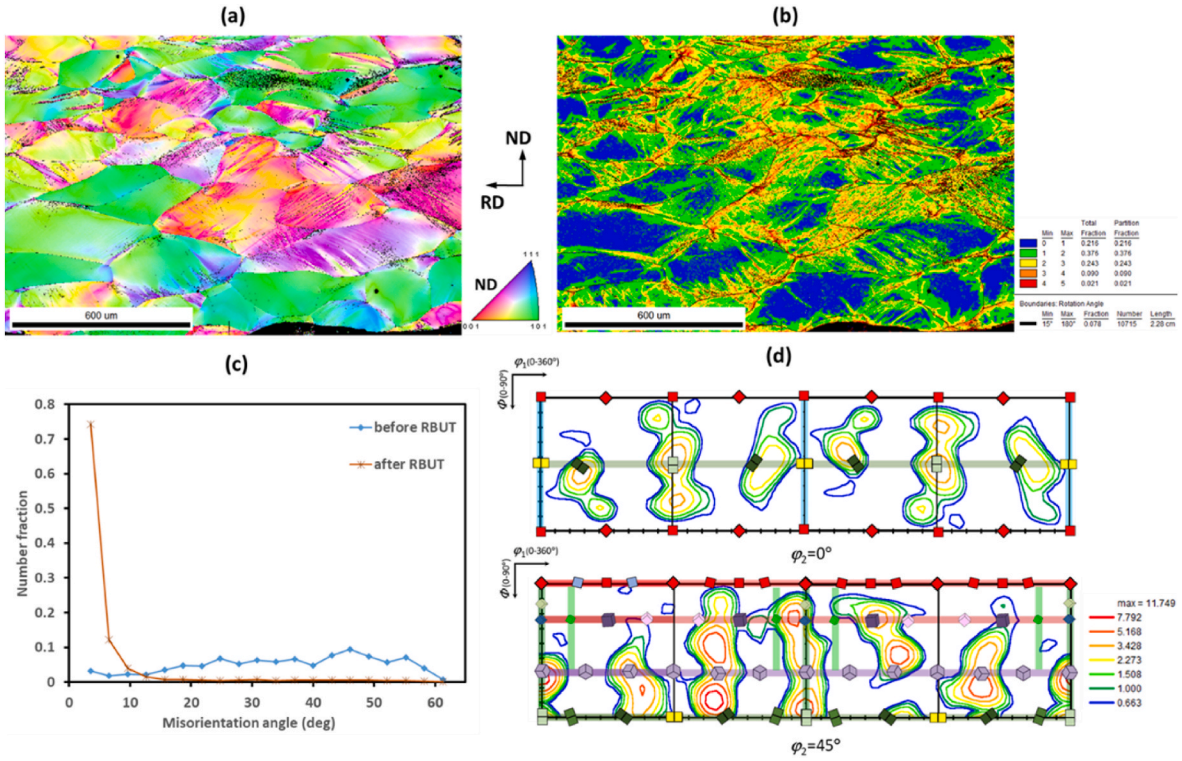

Fig. 7. EBSD results of the as R-BUT NOES sample: (a) IPF map (ND); (b) KAM map; (c) misorientation angle distribution, and (d) microtexture on the ODF sections of $\varphi_2 = 0°$ and $\varphi_2 = 45°$ (Bunge notation).

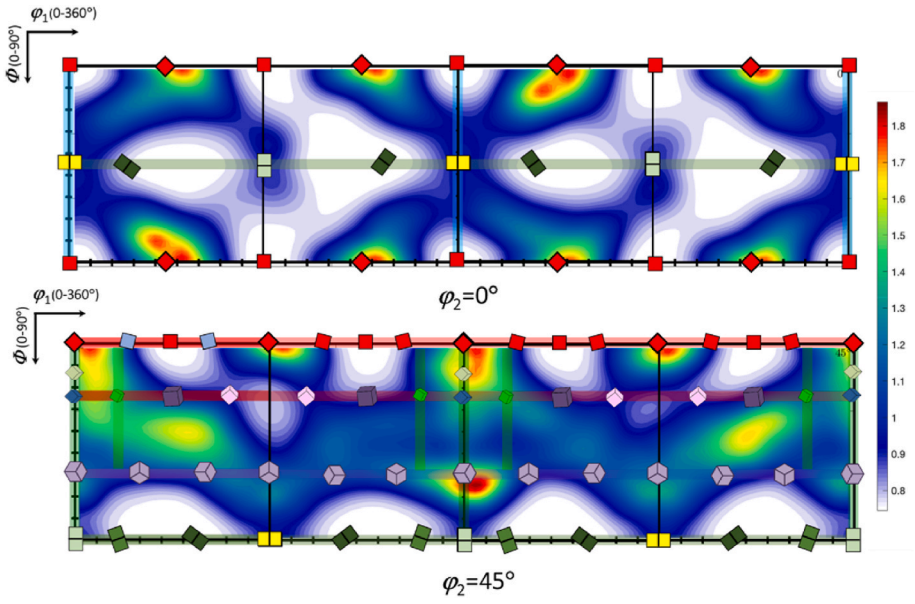

Fig. 8. Measured bulk texture using neutron diffraction: $\varphi_2 = 0°$ and $\varphi_2 = 45°$ of the sample subjected to R-BUT.

of grains (only about 30) covered by the microtexture measurement, which is not statistically significant.

In order to investigate the recrystallisation behaviour of the samples after R-BUT, partial recrystallisation annealing at 650 °C for 30 and 60 min was carried out, and the results are presented in Fig. 9a and Fig. 9b, respectively. Recrystallised and deformed grains are distinguished by the grain orientation spread (GOS) angle, i.e. those with GOS equal to or less than 3° are considered as recrystallised grains, while those greater than 3° are regarded as deformed grains [21]. Statistically, about 12.7% and 17.7% (area fraction) of the material has recrystallised after annealing for 30 and 60 min, respectively (Fig. 9c and d). The microtextures of the recrystallised grains after annealing at 650 °C for 30 and 60 min are presented in Fig. 9e and f, respectively. After 30 min, the new grains mainly show a brass ({110}<112>) texture, together with peaks at the cube ({001}<100>) and rotated cube ({001}<110>). After 60 min, the brass and cube textures are weakened, while the rotated cube is strengthened.

It is noted that a few cube crystals (5.4% area fraction within the recrystallised grains) nucleate in the sample after annealing for 30 min, which is rare in electrical steels after conventional rolling [6]. These

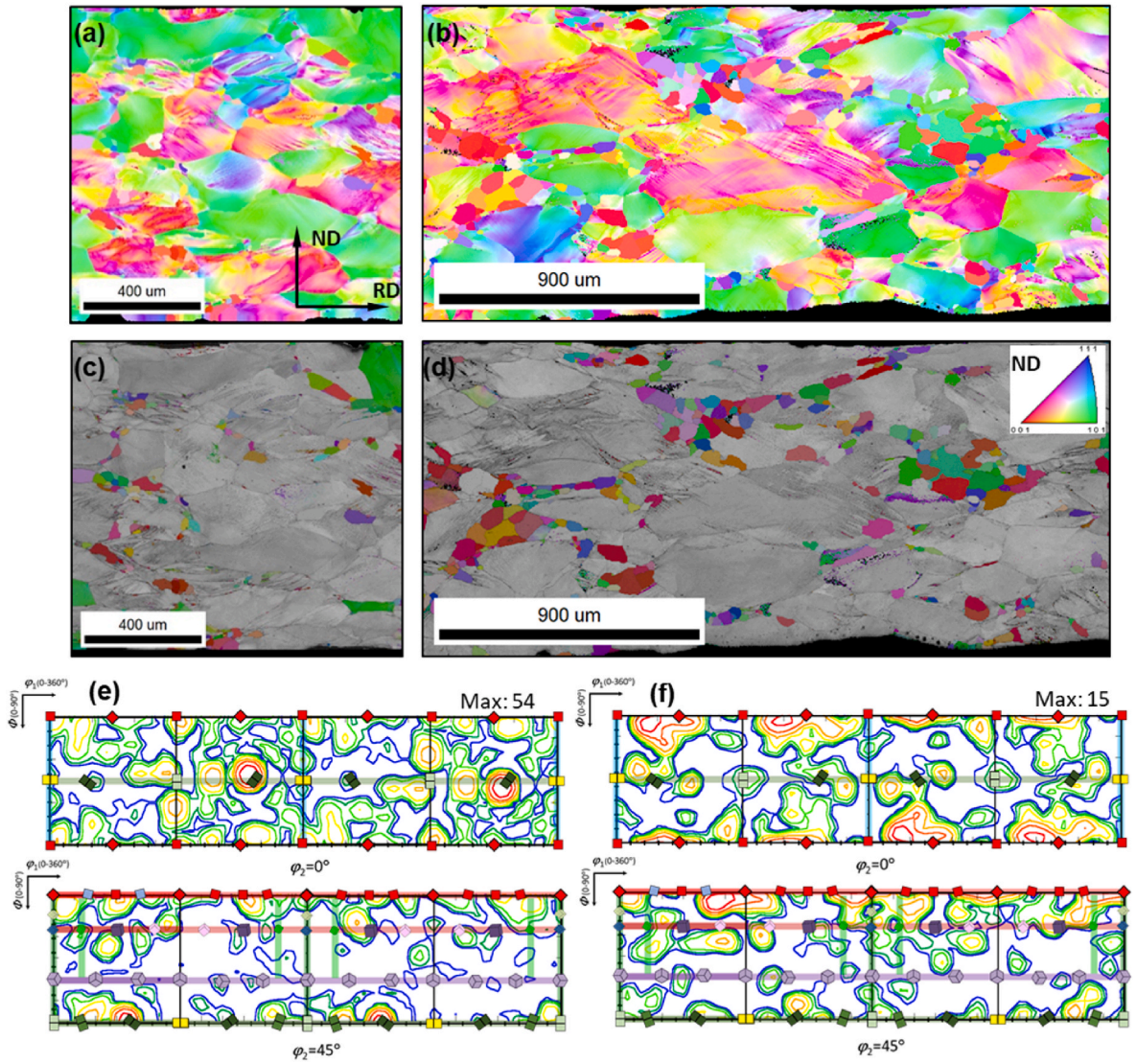

Fig. 9. Microstructures and microtextures of the R-BUT samples annealed at 650 °C: IPF maps after annealing for (a) 30 min and (b) 60 min; image quality maps after annealing for (c) 30 min and (d) 60 min; microtextures after annealing for (e) 30 min and (f) 60 min.

cube grains (with deviation angles of 8°–12° from the exact cube) are found near regions with non-uniform deformation (e.g., shear bands and deformation bands). These grains can nucleate from those substructures and grow by consuming the neighbouring deformed areas [6]. If the steel is annealed for 60 min, the area fraction of the cube grains is significantly reduced to only about 1.7%, while a larger amount of rotated cube grains (6.3% area fraction) form in the recrystallised microstructure.

For annealing at 750 °C, much of the microstructure is recrystallised after 10 min (Fig. 10). Annealing for longer time results in apparent grain growth. The GOS maps show that when the annealing time increases from 10 to 20 min and from 30 to 40 min, the area fraction of the recrystallised grains increases from 65% to 80% and from 87% to 91%, respectively. It is also noted that after 40 min, very large grains (diameter around 300 μm) appear in the microstructure, forming a bimodal distribution of both coarse and fine grains. To minimize the core loss, the grain size of the non-oriented electrical steels is ideally controlled at ~150 μm [1]; thus excessive grain growth should be retarded and avoided [22]. The distributions of the misorientation angles show that, the fraction of the low-angle boundaries (≤10°) in the deformed microstructure significantly drops, while that of the high-angle boundaries (≥20°) increases. For all the annealing times, the maximum fraction of the misorientation angles is at ~30°.

The microtextures obtained from the EBSD measurements are shown in Fig. 11. After annealing of the R-BUT processed samples for 10–30 min at 750 °C, the desired cube ({001}<100>), rotated cube ({001}<110>) and Goss ({011}<100>) components are strengthened. When the annealing time is less than 40 min, the maximum intensity of the ODF is about 6–7. After annealing for 40 min, the maximum intensity increases to about 12. The annealing textures of the R-BUT processed NOES are different from those after conventional rolling and annealing, although the initial textures are quite similar (i.e., mainly containing rotated cube, α-fibre, and γ-fibre). After rolling and annealing, the α-fibre and γ-fibre are usually retained, while after R-BUT and annealing, both the γ-fibre and the α-fibre are considerably weakened (e.g., after 40 min at 750 °C).

To quantitatively compare the textures, the volume fractions of the common texture components and fibres after annealing at 750 °C for various times are evaluated and presented in Fig. 12. Compared to the cold R-BUT material (Fig. 7), the volume fraction of the cube component is considerably increased by annealing for 10, 20, and 30 min, but it decreases when the annealing time is increased to 40 min. The volume fraction of the Goss component is also altered: annealing for 20 or 40 min significantly increases the volume fraction of Goss. The behaviour of

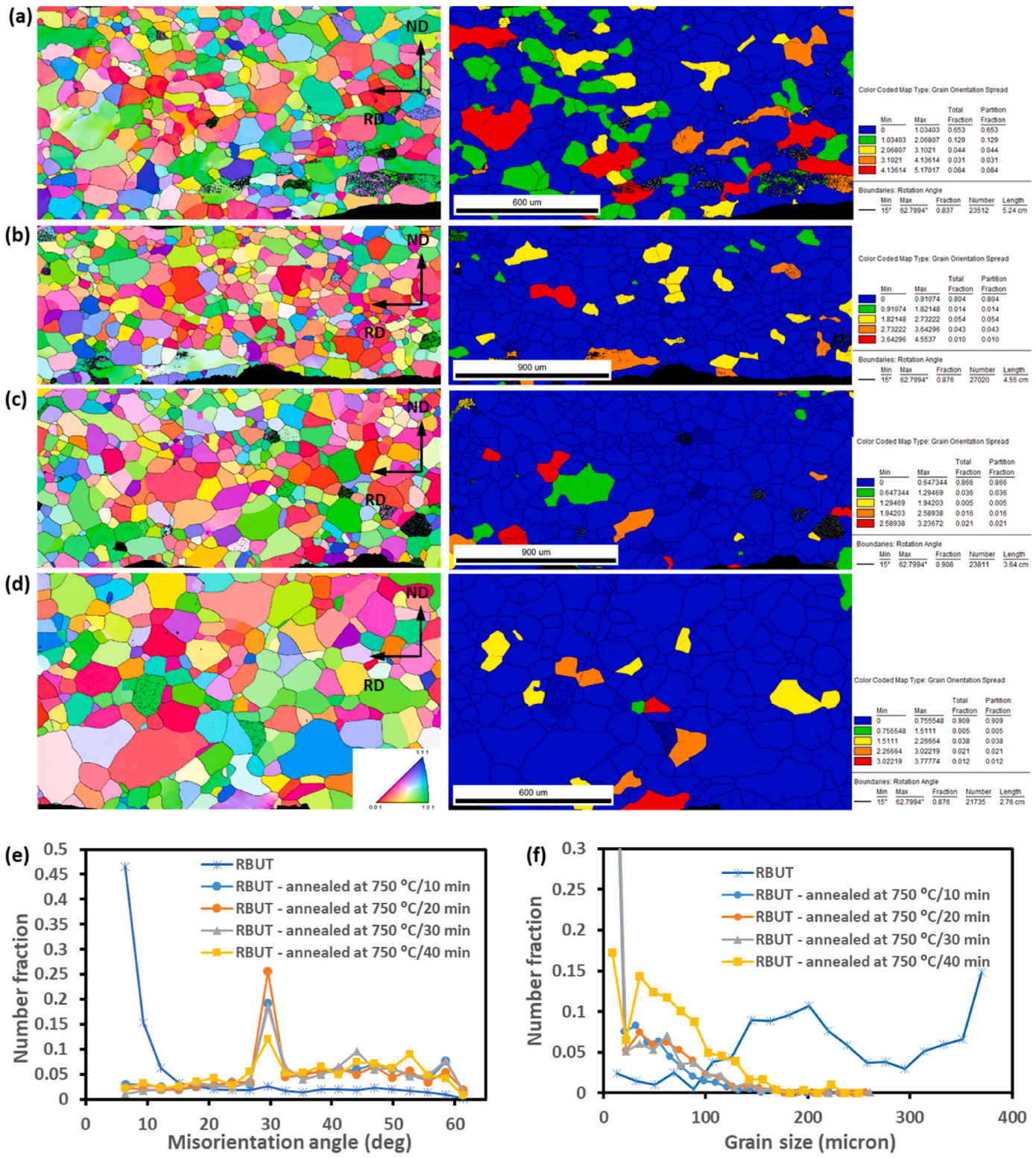

Fig. 10. Microstructure evolution after annealing at 750 °C for: (a) 10 min, (b) 20 min, (c) 30 min, (d) 40 min (IPF maps on the left and GOS maps on the right), (e) comparison of the misorientation angles, (f) comparison of the grain sizes.

the <111>//ND (γ-fibre) and <100>//ND (θ-fibre) textures is of particular interest. The volume fraction of the undesirable <111>//ND fibre after cold R-BUT was ~20%, which was significantly decreased to 10–13% through recrystallisation. On the other hand, the favourable <100>//ND fibre after cold R-BUT was ~2%, which reached to a maximum of ~9% after annealing at 750 °C for 30 min. Thus, annealing at 750 °C for 30 min would be an optimum heat treatment condition for this particular R-BUT deformation (i.e. $\omega = 400$ and d = 2 mm), as it promoted the desired θ-fibre while reducing the unfavourable γ-fibre. At this annealing time, the grain size is also within a suitable range for optimal core loss.

To evaluate the annealing macrotexture of the R-BUT processed

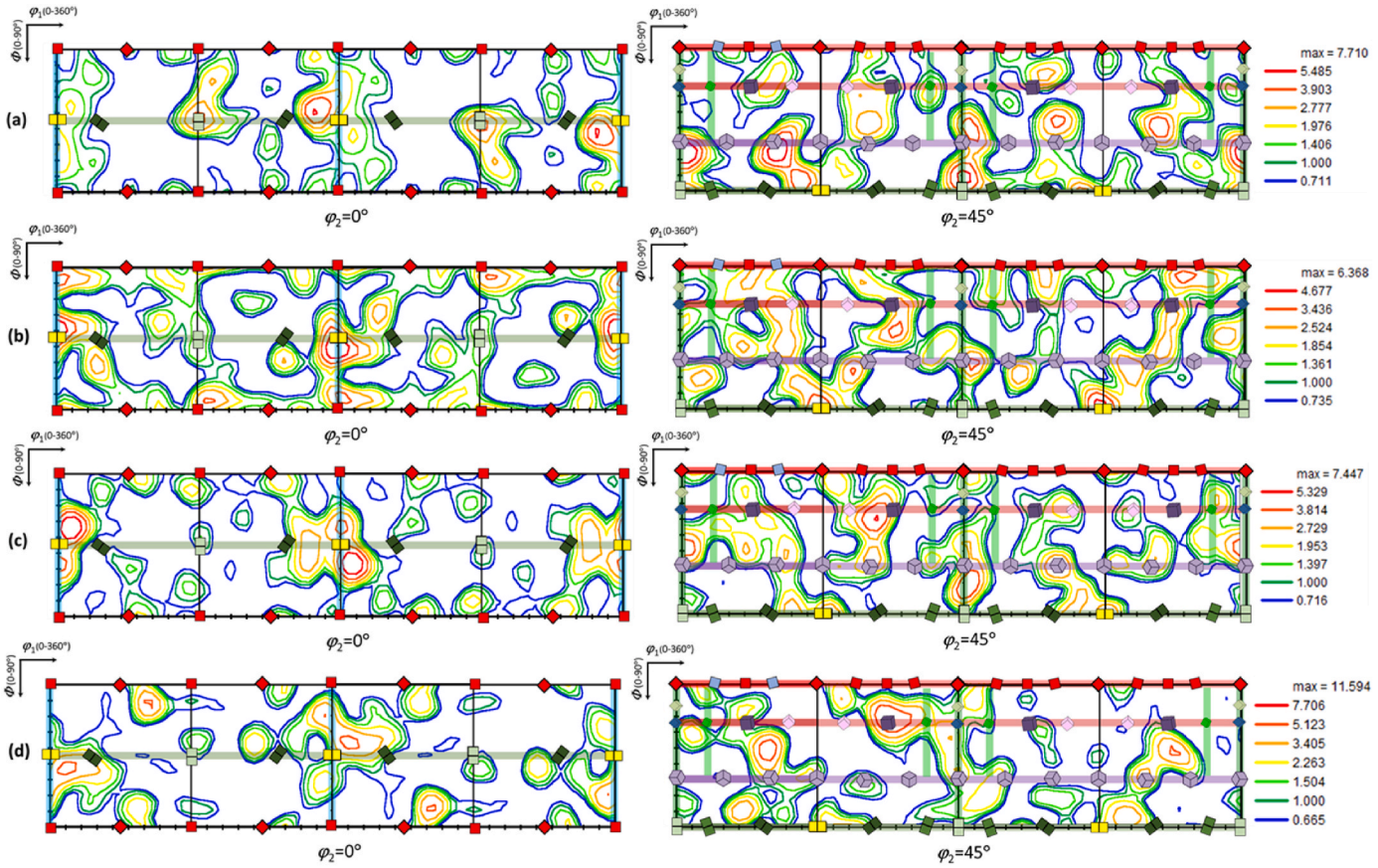

Fig. 11. Microtextures obtained by EBSD of the R-BUT sample subjected to annealing at 750 °C for: (a) 10 min, (b) 20 min, (c) 30 min, and (d) 40 min.

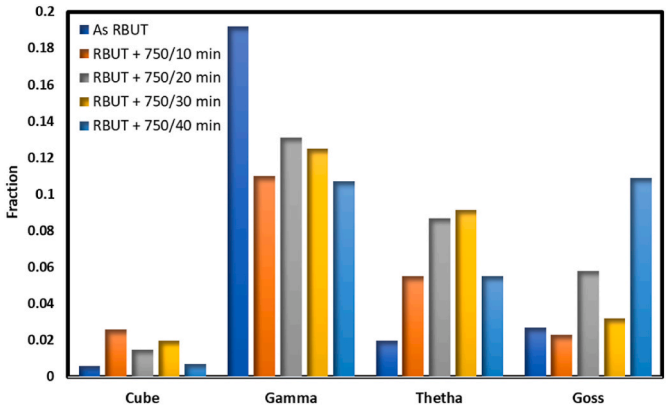

Fig. 12. Comparison of the volume fractions of prominent texture components and fibres after annealing at 750 °C for different times.

samples through the entire thickness, neutron diffraction technique was employed. As noted earlier, this is statistically more reliable texture measurement for these samples. Fig. 13 indicates the macrotexture of the R-BUT sample after annealing at 750 °C for 30 min. The dominant texture in this sample is the {001}<130> texture on the θ-fibre. The γ-fibre has been significantly reduced after recrystallisation.

4. Discussion

The mechanical responses of the electrical steel sheets subjected to R-BUT presented in Figs. 5 and 6 revealed that, in general, R-BUT can enhance the formability of the material. The deformation condition during the R-BUT process is similar to the deformation condition of the material under the incremental sheet forming (ISF) process. It has been shown [15] that, unlike a standard tensile test in which localised necking (responsible for failure) takes place right after defused necking, in the R-BUT operation, localised necking is postponed due to the special geometry of the bending assembly and the bending deformation on the R-BUT specimen. The enhanced formability of the R-BUT sample could be attributed to the negative triaxiality in the R-BUT operation. At the contact area between the rollers and the sample surface, stress triaxiality decreases down to negative levels. This negative stress triaxiality could delay the fracture of the material [15]. Also, the results indicate that the material requires smaller tensile loads to deform under R-BUT in comparison with the standard tensile test.

The texture evolution of the electrical steel specimens after R-BUT and subsequent annealing were shown in Section 3.3. When comparing the recrystallisation texture after R-BUT to that after cold rolling (e.g. [4, 23]), it is noted that the undesired <111>//ND fibre is effectively supressed through the R-BUT processing. On the other hand, the desired <001>//ND fibre is strengthened due to the introduction of shear plastic deformation through R-BUT deformation [24], which is difficult to form using conventional thermomechanical operations (i.e. conventional cold rolling followed by annealing). After conventional cold rolling, <111>//ND and <110>//RD usually develop, which may be further strengthened after annealing, although {001}<110> (rotated cube) may also develop [25].

It is noticed that in the suggested asymmetric rolling (e.g. [3]), annealing also creates the <111>//ND texture with enhanced component around {111}<110>. It was reported that increasing the level of asymmetry in the ASR process can weaken the texture in general and make <111>//ND more uniform [26]. In addition, it has been reported that annealing of asymmetrically rolled steel can also develop <001>//ND fibre texture [22]. It is shown here that this fibre has also

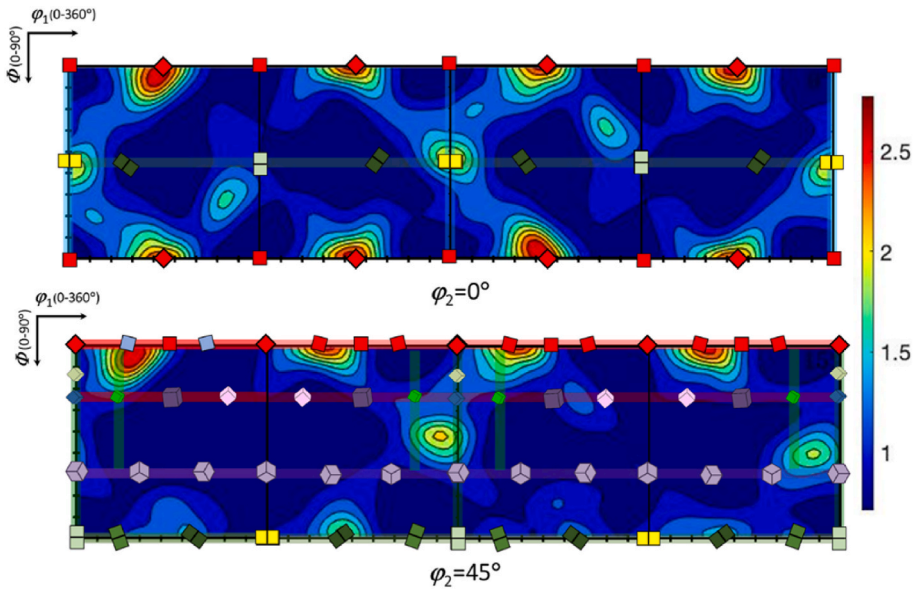

Fig. 13. Measured macrotexture using neutron diffraction: $\Phi_2 = 0°$ and $\Phi_2 = 45°$ of the R-BUT sample subjected to annealing at 750 °C for 30 min.

been strengthened through the recrystallisation of the R-BUT sample. It is seen that R-BUT can be more effective than asymmetric rolling in developing the favourable texture for magnetic applications. One of the reasons for this is that the level of shear plastic deformation introduced through asymmetric rolling relies on the friction between the rolls and the sheet surfaces, which is difficult to control and for many cases difficult to implement in an industrial processing line. Whereas in the R-BUT operation, the shear plastic deformation relies on the geometry of the rollers, which can be readily controlled and optimized.

5. Conclusions

NOES plates containing 1.8 wt% Si were subjected to repetitive bending under tension (R-BUT) deformation and subsequent annealing treatment. The mechanical behaviour, the microstructure and the crystallographic texture were characterized. The main findings are summarized as follows:

- NOES sheets can be deformed far beyond its common elongation limit using R-BUT operation. This may provide a solution to an important industrial challenge when processing NOES with extremely poor formability, e.g. electrical steels containing very high silicon.
- The undesired {111} texture can be significantly reduced through annealing after R-BUT deformation, while the desired {001} texture can be considerably enhanced, which makes R-BUT an interesting deformation process to optimize the crystallographic texture of NOES.
- The formation of cube texture in the R-BUT deformed electrical is also noted, which is usually difficult to develop through conventional rolling and recrystallisation. The shear plastic deformation induced in the R-BUT process is believed to cause the changes in texture after annealing.

CRediT authorship contribution statement

Saeed Tamimi: Conceptualization, Methodology, Formal analysis, Investigation, Visualization, Validation, Writing – original draft. **Youliang He:** Investigation, Formal analysis, Methodology, Validation, Writing – review & editing. **Mehdi Sanjari:** Investigation, Formal analysis, Validation, Writing – review & editing. **Hadi Pirgazi:** Investigation, Formal analysis, Validation, Writing – review & editing. **Winfried Kockelmann:** Investigation, Formal analysis, Writing – review & editing. **Fiona Robinson:** Validation, Writing – review & editing. **Mohsen Mohammadi:** Validation, Writing – review & editing. **Leo Kestens:** Validation, Writing – review & editing.

Declaration of competing interest

The authors declare that they have no known competing financial interests or personal relationships that could have appeared to influence the work reported in this paper.

Acknowledgements

The work has been supported by the Advanced Forming Research Centre (AFRC), University of Strathclyde (under the projects AFRC-CATP-1186 and AFRC-CATP-1390). The neutron data collection at the ISIS Neutron and Muon Source were supported by a beam time allocation RB2010728 from the STFC. Y.H. would like to acknowledge the financial support from Natural Resources Canada through the Program of Energy Research and Development. Erik Hilinski (Tempel Steel, USA) is thanked for providing the NOES plates.

References

[1] H. Shimanaka, Y. Ito, K. Matsumara, B. Fukuda, Recent development of non-oriented electrical steel sheets, J. Magn. Magn Mater. 26 (1–3) (1982) 57–64.
[2] R.F. de Araujo Cardoso, M.A. da Cunha, L.P.M. Brandão, Optimization of the magnetic losses of electrical steels through addition of Al and Si using a hot dipping process, J. Mater. Res. Technol. 2 (3) (2013) 276–281.
[3] S. Chen, J. Butler, S. Melzer, Effect of asymmetric hot rolling on texture, microstructure and magnetic properties in a non-grain oriented electrical steel, J. Magn. Magn Mater. 368 (2014) 342–352.
[4] L. Kestens, S. Jacobs, Texture Control during the Manufacturing of Nonoriented Electrical Steels. Texture, Stress, and Microstructure, 2008, 2008.
[5] Y. He, E. Hilinski, J. Li, Texture evolution of a non-oriented electrical steel cold rolled at directions different from the hot rolling direction, Metall. Mater. Trans. 46 (11) (2015) 5350–5365.
[6] M. Mehdi, Y. He, E.J. Hilinski, L.A. Kestens, A. Edrisy, The evolution of cube ({001}< 100>) texture in non-oriented electrical steel, Acta Mater. 185 (2020) 540–554.
[7] Y. He, E.J. Hilinski, Skew rolling and its effect on the deformation textures of non-oriented electrical steels, J. Mater. Process. Technol. 242 (2017) 182–195.
[8] M. Sanjari, Y. He, E.J. Hilinski, S. Yue, L.A. Kestens, Development of the {113}< uvw> texture during the annealing of a skew cold rolled non-oriented electrical steel, Scripta Mater. 124 (2016) 179–183.

[9] J. Sidor, R.H. Petrov, L.A. Kestens, Deformation, recrystallization and plastic anisotropy of asymmetrically rolled aluminum sheets, Mater. Sci. Eng.: A 528 (1) (2010) 413–424.
[10] S. Tamimi, J.P. Correia, A.B. Lopes, S. Ahzi, F. Barlat, J.J. Gracio, Asymmetric rolling of thin AA-5182 sheets: modelling and experiments, Mater. Sci. Eng.: A 603 (2014) 150–159.
[11] S. Tamimi, J.J. Gracio, A.B. Lopes, S. Ahzi, F. Barlat, Asymmetric rolling of interstitial free steel sheets: microstructural evolution and mechanical properties, J. Manuf. Process. 31 (2018) 583–592.
[12] W. Emmens, A.H. van den Boogaard, Incremental forming by continuous bending under tension—an experimental investigation, J. Mater. Process. Technol. 209 (14) (2009) 5456–5463.
[13] M. Zecevic, T.J. Roemer, M. Knezevic, Y.P. Korkolis, B.L. Kinsey, Residual ductility and microstructural evolution in continuous-bending-under-tension of AA-6022-T4, Materials 9 (3) (2016) 130.
[14] W. Emmens, A.H. van den Boogaard, An overview of stabilizing deformation mechanisms in incremental sheet forming, J. Mater. Process. Technol. 209 (8) (2009) 3688–3695.
[15] S. Tamimi, G. Sivaswamy, M.A. Siddiq, S. Rahimi, A. Leacock, P. Blackwell, Mechanical response and microstructure evolution of commercially pure titanium subjected to repetitive bending under tension, Mater. Des. (2020) 108814.
[16] W. Kockelmann, L. Chapon, P. Radaelli, Neutron texture analysis on GEM at ISIS, Phys. B Condens. Matter 385 (2006) 639–643.
[17] H.-R. Wenk, L. Lutterotti, S. Vogel, Rietveld texture analysis from TOF neutron diffraction data, Powder Diffr. 25 (3) (2010) 283–296.
[18] R. Hielscher, H. Schaeben, A novel pole figure inversion method: specification of the MTEX algorithm, J. Appl. Crystallogr. 41 (6) (2008) 1024–1037.
[19] A. Hadoush, A.H. van den Boogaard, W. Emmens, A numerical investigation of the continuous bending under tension test, J. Mater. Process. Technol. 211 (12) (2011) 1948–1956.
[20] T. Nguyen-Minh, J. Sidor, R. Petrov, L. Kestens, Occurrence of shear bands in rotated Goss ({1 1 0}< 1 1 0>) orientations of metals with bcc crystal structure, Scripta Mater. 67 (12) (2012) 935–938.
[21] S.W. Cheong, H. Weiland (Eds.), Understanding a Microstructure Using GOS (Grain Orientation Spread) and its Application to Recrystallization Study of Hot Deformed Al-Cu-Mg Alloys. Materials Science Forum, Trans Tech Publ, 2007.
[22] Y. Sha, F. Zhang, S. Zhou, W. Pei, L. Zuo, Improvement of recrystallization texture and magnetic property in non-oriented silicon steel by asymmetric rolling, J. Magn. Magn Mater. 320 (3–4) (2008) 393–396.
[23] O. Engler, V. Randle, Introduction to Texture Analysis: Macrotexture, Microtexture, and Orientation Mapping, CRC press, 2009.
[24] S. Tamimi, G. Sivaswamy, H. Pirgazi, B.S. Amirkhiz, S. Moturu, M.A. Siddiq, et al., A new route for developing ultrafine-grained Al alloy strips using repetitive bending under tension, Mater. Des. 206 (2021) 109750.
[25] M. Hölscher, D. Raabe, K. Lücke, Rolling and recrystallization textures of bcc steels, Steel Res. 62 (12) (1991) 567–575.
[26] A. Wauthier, H. Regle, J. Formigoni, G. Herman, The effects of asymmetrical cold rolling on kinetics, grain size and texture in IF steels, Mater. Char. 60 (2) (2009) 90–95.